

Origins Vs. fingerprints of the Jahn-Teller effect in d-electron ABX₃ perovskites

J. Varignon^{1,2}, M. Bibes¹ and Alex Zunger³

¹*Unité Mixte de Physique, CNRS, Thales, Université Paris Sud, Université Paris-Saclay, 91767, France*

²*Laboratoire CRISMAT, CNRS UMR 6508, ENSICAEN, Normandie Université, 6 Bd Maréchal Juin, F-14050 Caen Cedex 4, France*

³*Energy Institute, University of Colorado Boulder Colorado 80309, Boulder, CO, USA*

The Jahn-Teller (JT) distortion that can remove electronic degeneracies in partially occupied states and results in systematic atomic displacements is a common underlying feature to many of the intriguing phenomena observed in 3d perovskites, encompassing magnetism, superconductivity, orbital ordering and colossal magnetoresistance. Although the seminal Jahn and Teller theorem has been postulated almost a century ago, the origins of this effect in perovskite materials are still debated, including propositions such as super exchange, spin-phonon coupling, sterically induced lattice distortions, and strong dynamical correlation effects. Although the *end-result* of JT distortions often include a mix of such various contributions, due to coupling of various lattice, spin, and electronic modes with the distortions (“fingerprints”, or “consequences” of JT), it is not clear what is *the primary cause*: Which cases are caused by a pure electronic instability associated with degeneracy removal, as implied in the Jahn-Teller theorem, and which cases originate from other causes, such as semiclassical size effects. Here, we inquire about the *origin and predictability* of different types of octahedral deformation by using a Landau-esque approach, where the orbital occupation pattern of a symmetric structure is perturbed, finding if it is prone to total-energy lowering electronic instability or not. This is done for a systematic series of ABX₃ perovskite compounds having 3d orbital degeneracies, using the density functional approach. We identify (i) systems prone to an electronic-instability (a true JT effect), such as KCrF₃, KCuF₃, LaVO₃, KFeF₃ and KCoF₃, where the instability is independent of magnetic order, and forces a specific orbital-arrangement that is accommodated by a BX₆ octahedral deformation with a specific symmetry. On the other hand, (ii) compounds such as LaTiO₃ and LaMnO₃ with delocalized d states do not show any electronically driven instability. Here, their octahedral deformation mode results from coupling of lattice mode with semiclassical size-effects (sterically induced), such as BX₆ octahedra rotations. (iii) Although RVO₃ (R=Lu-La, Y) perovskites exhibit similar hybridizations as LaTiO₃, their t_{2g}² electronic structure is highly unstable and

preserves the Jahn-Teller effect. However, here coexisting steric deformations and JT distortions result in strongly entangled spin-orbital properties. This work provides a unified and quantitative DFT explanation of the experimentally observed trends of octahedral deformations in ABX_3 perovskites, without recourse to the dynamically correlated vision of electron interactions codified by the Mott-Hubbard mechanism.

I. Introduction

ABX_3 ($X=O, F$) perovskites^{1,2} show a number of systematic atomic distortions relative to the ideal cubic perovskite structure: the one made of corner-sharing, vertically positioned, all parallel BX_6 octahedra with equal B-X bonds. The interpretation of much of the electronic and magnetic phenomenology surrounding such perovskites^{1,2}, including superconductivity, colossal magnetoresistance, orbital ordering and metal-insulator transitions is intimately related to the understanding of the *causes vs. consequences* of the observed atomic distortions. Usually, distortion in ABX_3 perovskites produce inequivalent B-X bonds length, such as the Q_2 motion (*cf.* Figure 2 of Ref.³) that differentiate bond length along the x and y directions. These exist either as in-phase motions in consecutive planes along the z-axis (here labelled Q_2^+ motion, Fig1.c) or as in anti-phase along -z (here labelled Q_2^- motion, Fig1.d). Although octahedral deformations tilts (e.g., the in-phase ϕ_z^+ and anti-phase ϕ_z^- , displayed in Fig1.a, b) in different ABX_3 compounds are often similarly looking, they might have different origins. Possibilities include being (i) a consequence of the classic *size mismatch* between the A, B, and X atoms, as reflected by geometrical packing constructs such as the Goldschmidt tolerance factor⁴, or (ii) a true Jahn-Teller (JT)^{1,3,5,6} effect, reflecting an *electronic instability* associated with partial occupation of degenerate states, as described in the seminal work of Jahn and Teller⁶. Understanding predictively the causes of the observed displacements is central to interpreting numerous related phenomena *e.g.* gap formation due to symmetry lowering, metal-insulator transitions⁷, “orbital-orderings”⁸⁻¹⁰ and magnetic interactions¹¹ in ABX_3 perovskites. This is important since controlling octahedra deformations by using temperature, ferroelectricity, strain engineering or heterostructures¹²⁻¹⁹, may offer much needed knobs to control electronic devices.

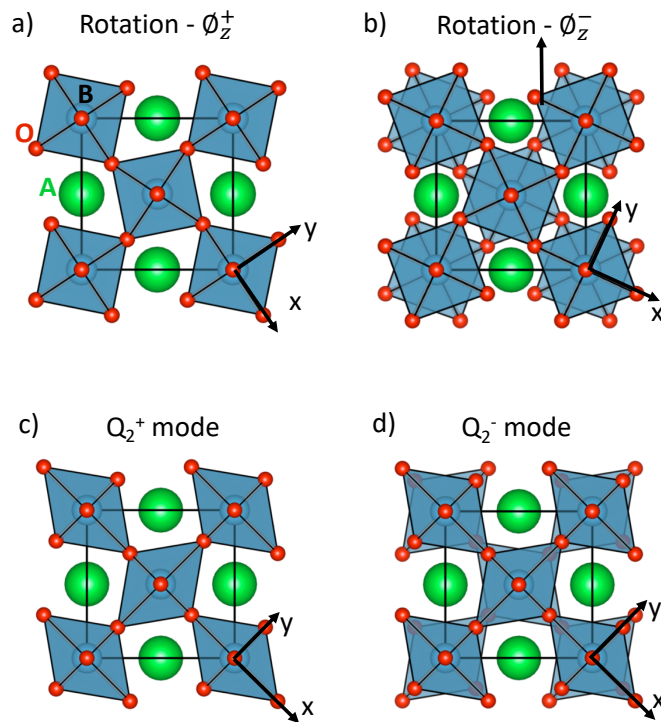


Figure 1: Sketches of the key lattice distortions appearing in ABX_3 materials. a and b) In phase (ϕ_z^+ , a) and anti-phase (ϕ_z^- , b) octahedral rotations around the z axis. c and d) Octahedral deformations propagating in phase (Q_2^+ , c) or in anti-phase (Q_2^- , d) along the z axis.

Puzzles: Predictive understanding of the mechanisms of octahedral distortions is rather challenging, for a number of reasons:

(a) Compounds with the same degenerate electronic configurations such as $KCrF_3$ ²⁰, $KCuF_3$ ²¹ and $LaMnO_3$ ²² being all e_g^1 ; or YVO_3 and $LaVO_3$ being both t_{2g}^2 (Ref. ²³) show different types of octahedral deformations at low temperature: Q_2^- for $KCrF_3$, $KCuF_3$ or $LaVO_3$, and Q_2^+ for YVO_3 and $LaMnO_3$, raising the question of what creates Q_2^+ and what creates Q_2^- ;

(b) Recent theoretical works predicted the surprising appearance of strong in-phase Q_2^+ symmetry-lowering octahedral deformations in compounds such as $SrTiO_3$, $BaMnO_3$ or $BiFeO_3$ even when there are no degenerate states (t_{2g}^0 , t_{2g}^3 or $t_{2g}^3e_g^2$ configurations, respectively)^{14,24};

(c) The textbook depiction of the JT force is often based on calculations based on the degenerate *orbital alone*, but one must consider the force resulting from the systems total energy, including not only the sum of one-electron orbital energy but also the electron-electron Coulomb and exchange-correlation energies resulting from degeneracy removal.

Literature models for explaining the origin of octahedral deformations in ABX₃ materials span a large range of mechanisms, including electronic super-exchange as codified by the Kugel-Khomskii model^{10,11}, electron-phonon coupling^{9,25}, lattice mode couplings involving rotations and forcing the Q₂⁺ mode^{13,26,27}, or specific dynamical correlation effects^{28,29}. The Kugel-Khomskii approach represents a phenomenological approach to understand the connection between orbital and spin order. However, it does not identify electronic and structural origins of what is a Jahn-Teller effect in perovskite, since both Q₂⁺ and Q₂⁻ modes are equally assumed to be JT distortions. Regarding the crucial role of dynamical correlations on the stabilization of JT distortions in perovskites, previous work claimed that *LDA and GGA* “usually fail to predict the correct electronic and structural properties of materials where electronic correlations play a role”⁹, similar statements also abound in literature^{9,28,29}. Nevertheless, such a belief was often grounded on a naïve implementation of DFT using either non-spin polarized simulations, and/or lack of symmetry breaking modes and use of simple exchange-correlation functionals that do not distinguish occupied from unoccupied orbitals. Recent works^{30–33} have clarified the fact that strong dynamical correlations are not the determining factor neither for gap opening nor for symmetry lowering displacements in ABO₃ materials.

Since none of these existing models or visions to explain JT distortions have been applied to a full range of ABX₃ compounds with different e_g-like and t_{2g}-like orbital occupations, at this time it is not clear if different mechanisms are needed to explain different distortions in different compounds, if Q₂⁺ and Q₂⁻ modes really reflect Jahn-Teller effects and if there is a basic theoretical framework that could explain them all.

Distinguishing features of the current approach: We address this subject by studying several ABX₃ materials (X=O, F) with a transition metal element exhibiting degenerate states (but without propensity to undergo disproportionation effect) using mean field like Bloch periodic DFT band theory with two stipulations. First, a polymorphous representation of the real space structure that permits the existence of different local environments to atoms and spins is required. This entails using crystallographic cells that are not limited to the smallest primitive cell, and therefore allow orbital, spatial and spin symmetry breaking, should these modes lower the total energy. Second, breaking orbital symmetries of degenerate partners requires an exchange correlation functional that distinguishes occupied from unoccupied

states, thereby affording significant cancellation of the self-interaction error and thus spatial compactness of 3d orbitals. Here we use DFT+U, (but nonzero U is not essential, as other exchange correlation functional make no use of an explicit U term³⁰). This approach provides DFT with a fair opportunity to reveal if the different patterns of symmetry breaking—spin order; JTD and /or ORT, and orbital occupation symmetry breaking—lower the energy or not, thereby establishing a first-principles framework for predictive theory of displacements in ABX₃ perovskites.

A Landau-esque perturbation approach: To determine if a potential deformation has electronic origin or not we use a Landau-esque perturbation approach that examines whether symmetry lowering via nudged occupation numbers in a degenerate manifold of an initially high symmetry cubic cell lowers the total energy or not. We examine the total energy for a number of prototypical cases encountered in 3d ABX₃ compounds: (a) equal occupations scenario of a degenerate level [such as (1/2, 1/2) for a single electron in doubly occupied e_g level] and (b) Orbital Broken Symmetry (OBS) scenario of degenerate partners, *e.g.* (1, 0). If (b) gives total energy lowering relative to (a) this signals the propensity for an electronic instability in the parent high symmetry phase, which is then followed up by the complete relaxation of the unit cell displacements, providing our predicted JT distortions (possibly with coupling to octahedral tilting). If the unequal occupations configuration (b) returns to the equal occupation configuration (a) during self-consistent calculation, this indicates that the high symmetry system is electronically stable and thus not prone to develop an *electronically enforced* JT distortion. Distortions present may reflect other factors such as the classic steric effects induced by size mismatch.

The main conclusions:

(a) The existence of electronic instabilities, *i.e.* a true JT effect is predicted in the high symmetry Pm-3m cubic phase of several ABX₃ compounds (KCrF₃, KCuF₃, LaVO₃, KFeF₃ and KCoF₃) whereas LaMnO₃ or LaTiO₃ have no such instability. Instabilities are manifested by breaking of orbital degeneracies while lowering the total energy, and thereby concomitantly opening finite band gaps.

(b) “Orbital-ordering” is always found to be a total energy lowering event. In such a state, electrons occupy an orbital that is pointing to orthogonal directions between all nearest-neighbor 3d atoms, such as alternation of d_{xy}/d_{yz} orbitals for a material with a t_{2g} degeneracy

or alternation of d_{y^2/dx^2} orbitals for a material with an e_g level degeneracy, thereby minimizing orbital interactions as codified by the phenomenological electronic super-exchange model of Kugel and Khomskii. The above observations are independent of the imposed magnetic ordering, thus substantiating the view the magnetic order is not the cause of the Jahn-Teller effect and related orbital-ordering, but rather a consequence of these phenomena.

(c) The Q_2^- octahedral deformation mode is a Jahn-Teller distortion: Following the identification of electronic instabilities in cubic cells, we follow the quantum mechanical forces to establish the fully relaxed crystal structures, finding that the aforementioned JT distorted compounds develop a Q_2^- octahedra deformation mode, which is therefore identified as an electronically induced Jahn-Teller distortion. The significance of the development of this specific Q_2^- mode is that it is characterized by *opposite* octahedral deformations between nearest sites and is thus able to accommodate the electronically induced orbital-ordering. Calculation of the magnitude of the displacements shows good agreement with the experimentally observed trends in a full range of ABX_3 compounds with t_{2g} and e_g degenerate partners

(d) At odds with the common perception, $LaMnO_3$ does not exhibit JT effect whereas $KCrF_3$ does, despite isovalent ($t_{2g}^3e_g^1$) configurations. Similarly, the t_{2g}^1 configuration $LaTiO_3$ has no JT distortion, whereas $KFeF_3$ does. This is because the existence of strong hybridization in the oxide cases diminishes orbital localization needed to create JT distortion, whereas in the fluoride the hybridization is much weaker.

(e) The Q_2^+ octahedral deformation, appearing in $LaMnO_3$ or $LaTiO_3$, is not induced by an electronic instability and thus it is not a Jahn-Teller distortion. It is a consequence of octahedral rotations and tilts often appearing in the perovskite oxides due to pure semiclassical atomic size effects, i.e. geometric steric effects. The Q_2^+ octahedral deformation mode thus cannot signal strong dynamical correlation effects in these ABX_3 compounds.

(f) Although $LaVO_3$ exhibits similar B, d – X, p hybridizations as $LaTiO_3$, the former compound exhibits a robust electronic instability in the cubic cell while $LaTiO_3$ has zero stabilization energy. The reason is that $LaVO_3$ has two electrons t_{2g}^2 relative to $LaTiO_3$ with just one t_{2g}^1 .

(g) Due to the coexistence of a JT effect and of octahedra rotations in RVO_3 materials, Q_2^- and Q_2^+ modes compete and result in two distinct spin-orbital orders at low temperature depending on the octahedra rotations amplitude.

(h) JT distortions as well as semiclassical size effect distortions can contribute to the opening of band gaps in Mott insulators. We have previously identified³³ four gapping modalities; the JT effect contributes just to modalities (iii) as follows: (i) compounds with closed subshells can open a gap due to octahedral crystal field splitting (CaMnO₃, LaFeO₃), (ii) compounds opening gaps by lifting degeneracies through large symmetry lowering displacements such as X₆ rotations (LaTiO₃ or LaMnO₃), (iii) compounds with two electrons in t_{2g} levels exhibiting Jahn-teller induced electronic instability able to cause gapping such as LaVO₃ (t_{2g}²e_g⁰) and (iv) compounds with unstable single local electronic occupation patterns disproportionating into a double local environment *e.g.* CaFeO₃ and YNiO₃.

We conclude that the electronically-induced Jahn-Teller distortion mode Q₂⁻ and the geometrically induced steric Q₂⁺ octahedral deformation mode are fully captured by a static mean-field method. This is in line with recent theoretical works that have demonstrated that static mean-field methods capable of inducing broken symmetry such as Density Functional Theory^{13,26,30,33} in a polymorphous representation suffice to also explain (i) the trends in gapping and type of magnetic order across the ternary ABO₃ series³³ and the binary 3d oxide series^{31,34}; (ii) the trends in disproportionation into two different local environments of the B site 2ABO₃ → A₂[B,B']O₆³² and (iii) the explanation of doping Mott insulators including cuprates^{35,36}, doping Kagome structures³⁷ as well as “anti-doping” oxides³⁸.

II. The elements of the method

The main features of the theoretical framework used in the study are as follows:

(a) Cell geometry and relaxation: We consider the following structure types: high symmetry Pm-3m cubic cell (LaTiO₃, LaVO₃, LaMnO₃, KFeF₃, KCoF₃, KCrF₃ and KCuF₃) as well as the experimentally observed structures, namely I₄/mcm (KCuF₃, KCrF₃), Pbnm (LaTiO₃, LaVO₃, LaMnO₃, LaTiO₃), P2₁/b (LaVO₃), I₂/m (KCrF₃), P-1 (KCoF₃) and I₂/a (KFeF₃) for identifying the DFT ground state structure. We allow cell sizes larger than the minimal (one formula unit per cell) so as to permit symmetry breaking distortions, should they lower the total energy. Atoms have to be nudged initially off their high symmetry positions in the cubic cell, followed by the calculation of the restoring Hellman Feynman forces guiding full

relaxation. In order to provide sufficient flexibility for developing general patterns of energy lowering deformations we have used a polymorphous crystallographic cell corresponding to a ($\sqrt{2}a, \sqrt{2}a, 2a$) cubic cell (*i.e.* 4 f.u per cell). The structural relaxation (lattice parameters and atomic positions) of ground state structures has also been performed until forces are lower than 1 meV/Å. We performed a symmetry adapted mode analysis that allows to extract the amplitudes of general distortion modes by projecting the distorted structure on the basis of the phonon eigen-displacements of the high symmetry cubic cell^{39,40}.

(b) Orbital symmetry breaking: The occupation numbers of partially filled degenerate orbitals in the high symmetry cubic cell is not restricted to equal occupations of the degenerate partners. For a compound with a single e_g electron, we do not pre-select a (1/2, 1/2) occupation pattern as generally done in standard band calculations, but allow also exploration of a (1,0) occupation pattern. Analogously, for 2 electrons in the t_{2g} level we explore (2/3, 2/3, 2/3) vs. (1,1,0) occupation patterns. Wave function symmetrization to a presumed symmetry is avoided so as to allow electrons to freely occupy energy lowering configurations. We therefore initially nudge not only atomic positions but also the occupation patterns of electrons in specific degenerate partners, called orbital broken symmetry states (OBS)^{41–43}. The self-consistent field with possible changes in d orbital occupancies is then obtained starting from this initial guess.

(c) Spin order: We use the observed low temperature spin order, *e. g.* AFMA (ferromagnetic planes coupled antiferromagnetically together), AFMC (AFM planes coupled ferromagnetically together) and AFMG (all nearest neighbor cations are antiferromagnetically coupled). Since we have previously shown that low temperature spin-ordered phase inherits the physics of the high temperature PM phase in ABO_3 materials³³, we did not attempt to model the PM distortions presently. For the study of the linear response of the ideal cubic phase, we prefer to use a simple FM order so as to avoid potentially strongly entangled spin-orbital situations as codified by the Kugel-Khomskii model^{10,11}, *i.e.* the chicken and the egg dilemma. This is reinforced by experimental observations of octahedra deformations appearing at higher temperatures than the AFM to PM (for example, in $KCrF_3$, $KCuF_3$, $LaMnO_3$).

(d) Exchange-correlation functional: To enable energy lowering occupations one needs to use an exchange-correlation (XC) functional that distinguishes occupied from unoccupied states. Local (LDA) and semi-local (GGA, meta-GGA) XC functionals do not make such

distinction. The simplest XC allowing this is DFT+U, where U is an on-site potential acting on a subset of orbitals – here the transition metal (TM) d states – and shifting to lower (upper) energies occupied (unoccupied) levels. We have thus employed this formalism in combination to the PBEsol⁴⁴ XC functional where U is an effective parameter $U_{\text{eff}}=U-J$.⁴⁵ We did not optimize the effective U values for each material to achieve an optimal fit (this might be done if needed in the future), but opt instead to use fixed $U=3.5$ eV for all 3d TM elements for simplicity.

III. Results

A. Examining the propensity of the symmetric structure for electronically-induced distortions

The Landau-esque symmetry breaking test perturbs a high symmetry cubic cell (here, Pm-3m with lattice parameter a_{cub}) and examines the total energy for (a) assumed equal occupations of the degenerate partners [no-OBS, such as (1/2, 1/2) for a single electron in doubly degenerate e_g level] and (b) Orbital Broken Symmetry (OBS), looking for energy lowering configurations [*e.g.* (1, 0)]. The spin configuration used is FM. Energy differences between these configurations are provided in Table I.

We see that given the opportunity for orbital broken symmetry, the compounds LaVO_3 , KFeF_3 , KCoF_3 , KCrF_3 and KCuF_3 show an energy gain $\Delta E_{\text{OBS-no/OBS}} < 0$, with a concomitant opening of the band gap, while LaTiO_3 and LaMnO_3 have $\Delta E_{\text{OBS-no/OBS}} = 0$, *i.e.* the initially imposed OBS relaxes back to configuration with equally occupied degenerate orbital, and the system stays metallic. These observations are unchanged by using another non-local functional such as HSE06^{46,47} hybrid functional method, having also a good adherence to self-interaction cancelation. It is significant that the sign of the energy difference is unaltered when one uses instead of the FM spin configuration the ground state magnetic order, namely AFMG for LaTiO_3 , KFeF_3 and KCoF_3 , AFMC for LaVO_3 and AFMA for LaMnO_3 , KCrF_3 and KCuF_3 , respectively, see numbers in parentheses in Table I.

| | Electronic configuration | (√2a _{cub} , √2 a _{cub} , 2 a _{cub}) cell (DFT+U) | | Primitive cubic cell (HSE06) |
|--------------------------|---|---|---------------------|--------------------------------------|
| | | ΔE _{OBS- no /OBS} (meV/f. u) | E _g (eV) | ΔE _{OBS- no /OBS} (meV/f.u) |
| LaTiO₃ | d ¹ (t _{2g} ↑ ¹) | 0 (0) | 0 | 0 |
| LaMnO₃ | d ⁴ (t _{2g} ↑ ³ e _g ↑ ¹) | 0 (0) | 0 | 0 |
| LaVO₃ | d ² (t _{2g} ↑ ²) | -297 (-237) | 0.42 | -428 |
| KFeF₃ | d ⁶ (t _{2g} ↑ ⁴ e _g ↑ ² t _{2g} ↓ ¹) | -655 (-873) | 1.78 | -780 |
| KCoF₃ | d ⁷ (t _{2g} ↑ ⁴ e _g ↑ ² t _{2g} ↓ ²) | -726 (-895) | 1.90 | -1071 |
| KCrF₃ | d ⁴ (t _{2g} ↑ ³ e _g ↑ ¹) | -124 (-85) | 0.66 | -256 |
| KCuF₃ | d ⁹ (t _{2g} ↑ ⁴ e _g ↑ ² t _{2g} ↓ ³ e _g ↓ ¹) | -71 (-81) | 0.38 | -477 |

Table I: Detection of spontaneous electronic instability in the high symmetry cubic phase of ABX₃ perovskites. Energy differences between solutions with equal occupancy of degenerate levels (no OBS) and with the most stable orbital broken symmetries (OBS) state in meV per formula units obtained in GGA+U and HSE06 functionals (the latter uses a smaller cubic cell for computational cost reason). The lattice parameter *a* is fixed to a relaxed cubic cell without OBS. A FM order is assumed. Results for the ground state AFM order is reported in parenthesis, namely AFMG for LaTiO₃, KFeF₃ and KCoF₃, AFMC for LaVO₃ and AFMA for LaMnO₃, KCrF₃ and KCuF₃, respectively.

1. The emergence of orbital order as a DFT total energy lowering Jahn- Teller effect

Once the degeneracies of the high symmetry phase are removed, one notes the creation of deterministic localization patterns of the degenerate partner components (such as d_{x²-y²} and d_{z²}) on different atomic sites. This “orbital ordering” has intrigued the community of 3d oxides^{3,11}, raising various exotic interpretations^{10,11,13,25–29}. To understand the possible unexotic, mean field total energy origins of such orbital ordering, we have investigated the energetics of different assumed orbital-arrangement: (a) electrons in the degenerate levels are initially nudged in *identical* orbitals on all nearest transition metal sites, such as a d_{z²} occupancy on all sites for a compound with a single e_g electron; (b) the electron is initially nudged in a *different* degenerate partner between nearest TM sites in the (xy) plane but on *the same* partner for TM located in the consecutive plane along the z direction, such as alternation of d_{x²} and d_{y²} in the (xy) plane with similar arrangement on the consecutive plane along z, thus forming a “columnar arrangement” and (c) the electron is initially nudged in a

different degenerate partner between *all* nearest neighbor site, such as alternation of d_x^2 and d_y^2 in all cartesian directions, thus forming a 3D checkerboard. For a compound with 2 unpaired electrons for t_{2g} levels, case (b) and (c) necessarily require that an identical orbital has to be occupied between nearest TM sites. We thus imposed one electron in a specific t_{2g} partner on all TM sites (d_{xy} here) and then we alternate the occupancy of the remaining partners (d_{xz}/d_{yz}). After initial nudging, (intended to avoid accidental local minimum), the solution is iterated to self-consistency with full relaxation of the electronic structure but without any structural relaxation.

The results show that for all compounds displaying a spontaneous electronic instability, *the lowest energy state is always associated with configuration (c) – e.g. alternation of d_x^2 and d_y^2 in all cartesian directions, thus forming a 3D checkerboard.* (The total energies of single, columnar and checkerboard OBS states are provided in Supplementary section I” Total energies of Orbital Broken Symmetry states in cubic cells”). In such a minimum energy state, electrons occupy an orbital that is pointing to orthogonal directions between all nearest-neighbor transition elements, such as alternation of d_{xy}/d_{yz} orbitals for a material with a t_{2g} degeneracy, or alternation of d_y^2/d_x^2 orbitals for a material with an e_g level degeneracy as shown by our partial charge density maps of states near the Fermi level (Fig 2.a, b, d and e). This specific pattern is referred to as a G-type antiferro-orbital ordering^{13,23,48} that minimizes orbital interactions between all nearest neighbor TM site on a perfectly cubic lattice. Significantly, these energy-lowering states all exhibit band gaps with respect to the cubic cell with equally occupied degenerate partners, even though no structural relaxation has been performed as yet (see Table I). *We conclude here that in $LaVO_3$, $KFeF_3$, $KCoF_3$, $KCrF_3$ and $KCuF_3$, the electronic structure in the cubic cell is distorting in order to remove the orbital degeneracy, thereby producing an antiferro-orbital arrangement and opening a band gap. These compounds therefore exhibit the signatures of a Jahn-Teller effect that is directly related to gapping.*

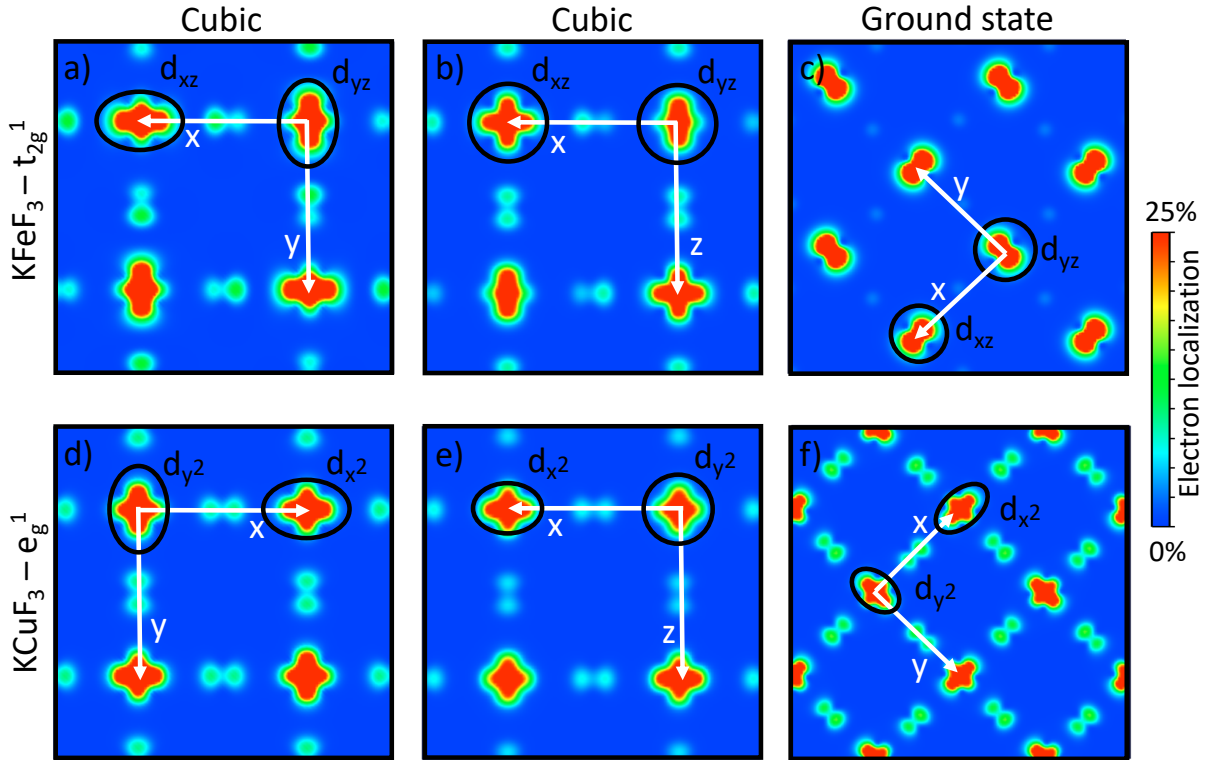


Figure 2: Orbital orderings appearing ABX_3 materials. Wavefunction squared maps of electrons located at the top of the valence bands (latest two occupied bands) for $KFeF_3$ (a, b and c) and $KCuF_3$ (d, e and f) in their unrelaxed cubic cells (a, b, d and e) and in the fully relaxed ground state structure (c and f).

2. When electronic delocalization of degenerate orbitals prevents the JT effect

One might wonder at this stage why compounds with identical electronic degeneracy differ in their ability to have a JT effect. For example, $LaMnO_3$ does not exhibit a JT effect whereas $KCrF_3$ does; similarly, $LaTiO_3$ has no JT effect, whereas $KFeF_3$ does. To understand this, let us recall that the energy surface of a JT system⁴⁹ as a function of a displacement x can be represented as $E(x) = -F_{JT}x + 1/2Kx^2$, consisting of a stabilizing electronic JT force F_{JT} associated with electronic degeneracy removal, and an opposing harmonic restoring force of the surrounding bond characterized by the force constant K . That the existence of degeneracy of partially-filled states does not automatically force a JT distortion is clear from the competition between these two terms: if the relevant (degenerate) orbitals are too hybridized/delocalized (weak F_{JT}), or the harmonic response of the bonds about to be deformed is too stiff, degeneracy will not lead to a JT distortion. Strongly (weakly) p-d hybridized systems will tend to have a weaker (stronger) JT force. To assess such tendencies, one must carry out a JT

distortion inspecting the total (electron-electron; electron-ion and ion-ion) energy terms, not just orbital energies. This is readily done in DFT supercell theory.

To assess the difference in hybridization between fluorides and oxides, Fig. 3 shows the projected density of states of isoelectronic pairs (LaTiO₃ vs. KFeF₃, as well as LaMnO₃ vs. KCrF₃) in the high symmetry cubic cell with equal occupancies of degenerate partners. As one can see, the fluorine-based compounds show minimal hybridizations between the B-d and X-p states, and the bandwidth associated with degenerate partners is rather narrow, thus resulting in a localized electronic structure and d-d like band edges. On the other hand, for oxygen-based perovskites, the hybridization between B-d and X-p states and the band width associated with degenerate partners increases continuously upon adding electrons to the d levels, until reaching a ‘charge transfer insulator’ regime for LaMnO₃ – *i.e.* anion p like VBM and cation d like CBM. This thus suggests that oxides have more delocalized d states than fluorides. Thus, in the oxides the JT force can be too weak and might be overcome by the restoring force but in the fluorides the JT force is stronger and might win. This is what we see in Table I.

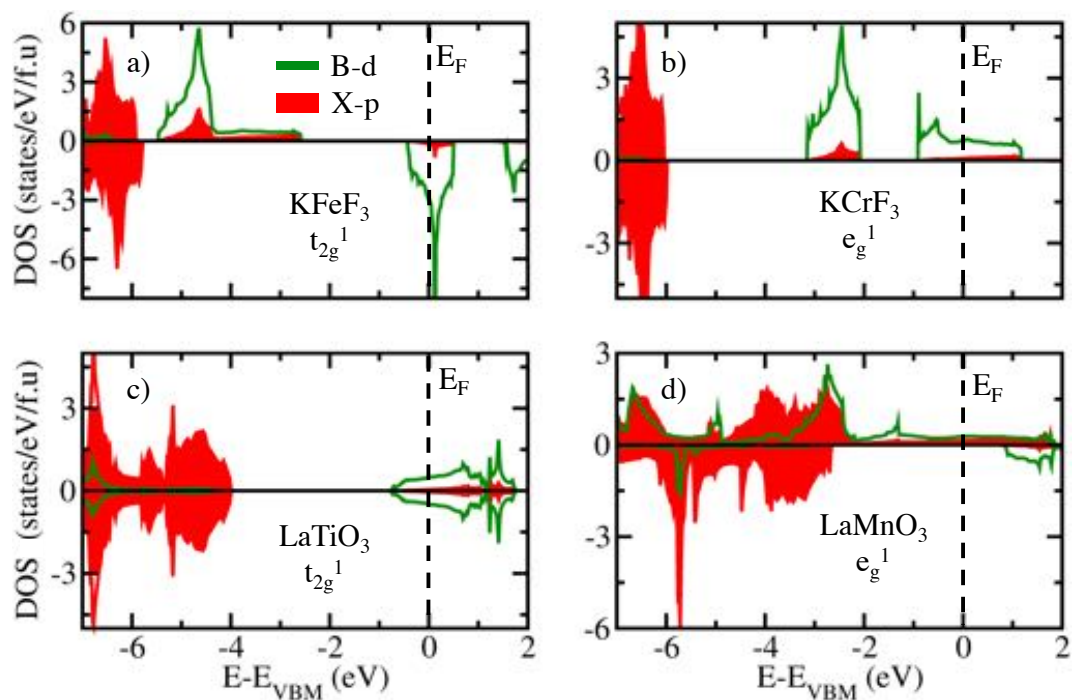


Figure 3: Electronic structure of compounds with isoelectronic degeneracies. Projected density of states on B-d (green) and X-(red) p states in materials showing a t_{2g} (KFeF₃ and LaTiO₃, panels a and c) and e_g (KCrF₃ and LaMnO₃, panels b and d) isoelectronic degeneracies in their cubic cell. The vertical line indicates the Fermi level. A simple FM order is used.

To next check how the degree of localization of degenerate orbitals induces JT displacements, we design enhanced localization in LaTiO₃ by increasing the lattice constant, *i.e.* using a (negative) hydrostatic pressure. Starting from this new cubic cell in which the bandwidth of the t_{2g} degenerate partners is reduced by 0.5 eV *wrt* the unperturbed cubic cell, we again nudge the Ti³⁺ electron to specific t_{2g} partners (see Supplementary Section II “Density of states of LaTiO₃ under negative pressure”). LaTiO₃ now develops a small electronic instability ($\Delta E_{\text{OBS-no OBS}} = -6$ meV/f.u) producing an antiferro-orbital occupancy between all nearest neighbor Ti³⁺ sites and opening a band gap of 0.1 eV. Therefore, upon decreasing B, d – X, p hybridizations and the t_{2g} levels bandwidth, LaTiO₃ undergoes a Jahn-Teller effect.

We conclude that delocalized degenerate states can prevent an electronic instability and the ensuing Jahn-Teller effect despite the presence of orbital degenerate states. This also explains why SrVO₃ or CaVO₃, showing strongly hybridized electronic structures, do not develop a JT effect and thereby stay metallic.

3. Trends in JT energies with orbital occupancy

Although LaVO₃ exhibits similar B, d – X, p hybridizations as LaTiO₃, the former compound possesses a robust electronic instability in the cubic cell (energy lowering of 297 meV; Table I), while LaTiO₃ has zero stabilization energy. This reflects the fact that the JT force is larger in systems with higher orbital occupancy – LaVO₃ with two electrons t_{2g}^{↑2} relative to LaTiO₃ with just one t_{2g}^{↑1}. Similarly, the energy gain associated with breaking orbital degeneracies increases when going from t_{2g}^{↑1} in KFeF₃ to a t_{2g}^{↑2} in KCoF₃. In general, we expect that triply degenerate states occupied by 2 electrons to have the greatest JT instability.

We next turn to study the trends in the deformation amplitudes.

B. The Q₂⁻ octahedral deformation mode is a Jahn-Teller distortion

1. Electronically unstable cubic structures develop the Q₂⁻ octahedral deformation upon relaxation

While literature often ascribe Q₂⁺ and Q₂⁻ modes to a JT effect^{2,3}, we inspect here the type of distortion forced by the spontaneous electronic instability in the hypothetical cubic

structure of LaVO_3 , KFeF_3 , KCoF_3 , KCrF_3 and KCuF_3 . To that end, we allow these systems to change their structures by fully developing energy lowering displacements. Application of structural relaxation techniques (following quantum mechanical forces to zero force configurations) reveals all these systems develop specifically the anti-phase Q_2^- octahedral deformation that we therefore consider as the fingerprint of JT effect in these systems. We tested the Q_2^+ octahedral deformation mode but this octahedral deformation mode produces lower energy gains than the Q_2^- mode (see Supplementary Section III "Energy gain associated with Q_2^+ and Q_2^- octahedra deformation mode").

Symmetry adapted mode analysis of the relaxed DFT structures (starting from experimentally observed structures and magnetic orders) are presented in Table II. One can appreciate the development of the specific Q_2^- mode by the presence of shifted single well potential energy surface associated with the Q_2^- mode starting from a cubic cell, signaling the presence of a Jahn-Teller force F_{JT} (see Supplementary Section IV "Potential energy surfaces associated with the Q_2^- "). Note that the shifted single wells are independent of the spin order – FM and AFM orders yield similar results—, and thus the magnetic order at low temperature may be a consequence of the specific orbital-orderings forced by the electronic instability, but not its cause. The significance of the development of this specific Q_2^- mode (Figure 1.d) is that it is characterized by *opposite* octahedral deformations between nearest sites, and is thus able to accommodate and amplifies the incipient orbital-orderings (Fig 2.c and f). Specifically, the B-X bonds expand and contract in the plane defined by the alternating directions of the occupied orbitals.

We emphasize that the appearance of an anti-phase rotation propagating orthogonally to the JT distortion leads to very small additional components to the symmetry allowed JT distortion in which apices O move inward/outward (Supplementary Section V explains "The anti-phase rotation and the Q_2^- motion displacements patterns describe orthogonal planes in KCrF_3 for minimizing electronic super-exchange"). Although it is sometimes proposed to come from additional electron interactions⁵⁰, it is just a consequence of the X_6 rotation (see Supplementary Section VI "Low temperature orbital and structural transition in KCrF_3 ").

2. Theory vs. experimental observation for the Q_2^- octahedral deformation mode

The predicted specific symmetry of the Q_2^- mode is precisely what is needed to explain the cubic to tetragonal I_4/mcm structural transition in $KCrF_3$ and $KCuF_3$ (observed at $T=973$ K and 800 K^{51,52}, respectively), and of the $Pbnm$ to $P2_1/b$ structural transition observed in RVO_3 compounds ($R=Lu-La, Y$)^{23,53}. Table II summarizes the calculated vs. experimental values of the amplitudes of the Q_2^- displacements, showing very good agreement.

| | t factor | Magnetic order | Space Group | Q_2^+ (M_3^+) Calculated (Exp.) | Q_2^- (R_3^-) Calculated (Exp.) |
|--------------------------|----------|----------------|-------------|--|--|
| LaTiO₃ | 0.93 | AFMG | $Pbnm$ | 0.040 (0.041 ⁵⁴) | - |
| LaMnO₃ | 0.94 | AFMA | $Pbnm$ | 0.324 (0.357 ²²) | - |
| LaVO₃ | 0.95 | AFMC | $P2_1/b$ | 0.005 (0.009 ⁵⁵) | 0.093 (0.079 ⁵⁵) |
| | | | $Pbnm$ | 0.078 (0.090 ⁵⁶) | - |
| KFeF₃ | 1.00 | AFMG | I_2/a | - | 0.104 (-) |
| KCoF₃ | 1.01 | AFMG | $P-1$ | - | 0.003 (-) |
| KCrF₃ | 0.99 | AFMA | I_2/m | - | 0.336 (0.316 ²⁰) |
| | | | I_4/mcm | - | 0.300 (0.299 ²⁰) |
| KCuF₃ | 1.03 | AFMA | I_4/mcm | - | 0.335 (0.355 ²¹) |

Table II: Amplitudes associated with structurally distorted octahedra in the ground state of ABX_3 perovskites. Amplitudes of distortions (in Å) associated with the Q_2^+ and Q_2^- modes (irreducible representations M_3^+ and R_3^- respectively) distorting octahedra of the optimized structures starting from a cubic cell with the A cation located at the corner of the cell. Experimental values extracted from structures available in literature are provided in parenthesis. The Goldschmidt t factor is also reported, as well as the magnetic state observed experimentally at low temperature and assumed in the simulation for the relaxation of the ground states.

C. The Q_2^+ motion in $LaTiO_3$ and $LaMnO_3$ is a consequence of classic octahedral rotations and tilting, not an electronic JT effect

Consistent with the absence of electronic instabilities in the high symmetry Pm-3m cubic cell of LaTiO₃ and LaMnO₃, we find that the Q₂⁺ or Q₂⁻ octahedra deformation are associated with a single well energy potential (see figures 4.a and b) and are unable to open a band gap. Such observations were already raised by Lee *et al* for LaMnO₃ in Ref.⁵⁷. This means that, although a sizable Q₂⁺ octahedra deformations mode appears in the ground state structure of LaTiO₃ and LaMnO₃, this mode is not produced by an electronic instability, does not lift orbital degeneracies or produce the metal-to-insulator transition, all being key aspects of the Jahn-Teller effect.

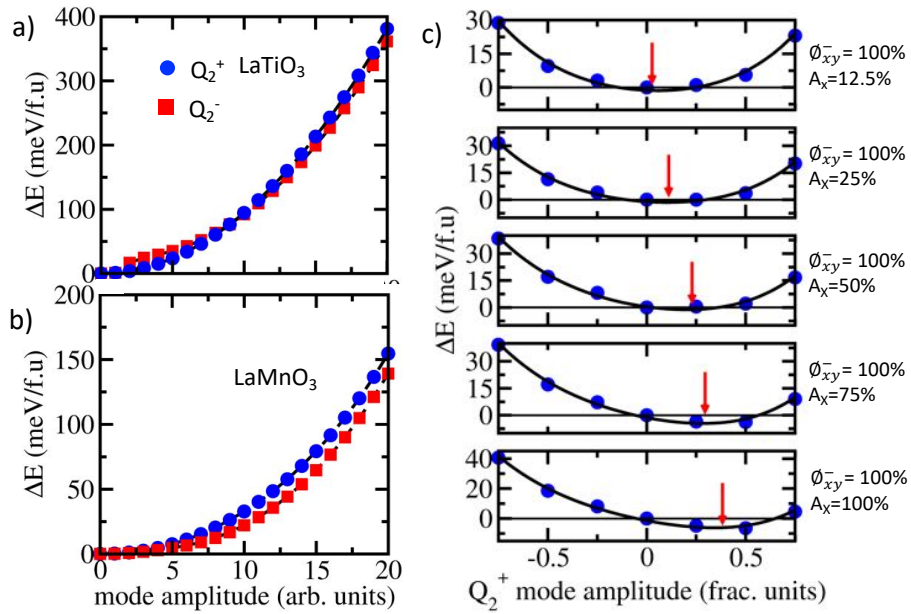


Figure 4: Induced Q₂⁺ motions through lattice mode couplings. a and b) Energy versus Q₂⁺ (filled blue circles) and Q₂⁻ (filled red squares) mode amplitudes (arbitrary units) in LaTiO₃ (a) and LaMnO₃ (b) using a FM order starting from a cubic cell. c) Energy difference (in meV/f.u) versus Q₂⁺ mode amplitude at fixed amplitude of ϕ_{xy}^- and A_x in LaMnO₃ using a FM order. 1 (100%) represents the amplitude appearing in the ground state. The reference energy is set at 0 amplitude of the Q₂ mode.

Nevertheless, these compounds develop two anti-phase and one in-phase X₆ rotations (due to low t factors, see Table II) that allow a specific lattice mode coupling between the Q₂⁺ mode plus the antiphase rotation ϕ_{xy}^- and the antipolar motion A_x (sketched in Fig 1. of Ref.²⁶) of the form $F \propto \phi_{xy}^- A_x Q_2^+$ in the free energy expansion as identified in Ref.¹³. The appearance of finite amplitudes of ϕ_{xy}^- and the A_x modes automatically forces finite amplitudes of the Q₂⁺ mode in order to lower the total energy as we see in Fig.4.c for LaMnO₃. A similar result is

found for LaTiO_3 (not shown). Although the dependence of the Q_2^+ mode on rotation amplitude in LaMnO_3 was already shown in Ref.⁵⁷, we show that the Q_2^+ is nothing but a consequence of ABX_3 distortions originating from pure steric atomic size effects captured already by the 1926 pre quantum Goldschmidt tolerance factor⁴. In analogy with improper ferroelectrics^{58,59}, the Q_2^+ mode can be thought of as an improper mode, being a result of a specific octahedra rotations pattern: a combination of two anti-phase and one in-phase rotations. In contrast to often articulated statements^{9,22,28,60,61} this Q_2^+ motion should not be confused with a JT distortion originating from an electronic instability. The improper mode origin of Q_2^+ is consistent with previous theoretical reports of strong Q_2^+ mode amplitude reported in compounds that lack degenerate levels¹⁴, clearly signaling that this mode cannot originate from an electronic instability.

1. The appearance of an Q_2^+ mode is not a statement of strong dynamical correlation effects

Leonov *et al*²⁸ highlighted the importance of dynamical correlations in stabilization of the Q_2^+ mode in LaMnO_3 . They plotted the potential energy surface as a function of the Q_2^+ mode amplitude with Dynamical Mean Field Theory (DMFT) simulations starting from a cell with rotations and the A_x mode, explaining that “*in the calculation we change only the parameter ∂_{JT} (i.e. the amplitude of the Q_2^+ mode) ... and keep the value of the MnO_6 octahedron tilting and rotation fixed*”. As can be seen by comparing our mean field DFT result of Fig 4.c with their DMFT results (Fig. 8 of Ref.²⁸), the two agree closely, suggesting that in this case, adding dynamic electronic correlations does not bring any new features to the understanding of the octahedra deformation in ABX_3 materials.

2. The origin of the improper Q_2^+ motion in LaMnO_3

Our first-principles results demonstrate that the Q_2^+ mode is a simple consequence of octahedra rotations, but one wonders if one can extract experimental evidences of this phenomena. At high temperature, LaMnO_3 adopts a rhombohedral R-3c phase that is characterized by an anti-phase rotation ϕ_{xyz}^- around all cartesian axes and in which no

octahedral deformation nor related phenomena such as an orbital-ordering are reported^{22,62}. This is compatible with our models since (i) no electronic instability yielding a Q_2^- JTD mode is identified in LaMnO_3 and (ii) such X_6 octahedra tilt pattern does not allow A_x and Q_2^+ modes to develop by symmetry. Once LaMnO_3 transforms to the Pbnm cell around 750 K, one observes that experimental structures at various temperature taken from Ref.²² develop an A_x distortion whose amplitude increases with decreasing temperature, *while ϕ_{xy}^- is not temperature dependent*. Upon increasing of the A_x mode amplitude on cooling, the Q_2^+ mode amplitude increases (See supplementary section VII “Symmetry Mode Analysis of LaMnO_3 experimental structures” for symmetry adapted modes of these structures). This thus confirms the “improper appearance” of the Q_2^+ octahedra distortion mode.

D. Competing Jahn-Teller effect and sterically induced Q_2^+ mode is at the core of the entangled spin-orbital properties in RVO_3 compounds

Although Q_2^+ and Q_2^- distortions have totally different origins, they can coexist as long as the Q_2^+ mode is allowed by symmetry. This is the case in LaVO_3 for which one observes finite amplitudes of the two modes in the low temperature phase both at the theoretical and experimental levels (see Table II), although the JT distortion largely dominates. However, among the RVO_3 (R=Lu-La, Y) compounds, LaVO_3 shows the smallest octahedra rotations. One may question *what happens for a compound showing larger X_6 rotations such as YVO_3 ?*

Consistently with previous literature^{13,53}, full structural relaxation (atomic position + cell parameters) of YVO_3 yields a Pbnm ground state showing only the Q_2^+ mode at 0 K. Interestingly, through appearance of the Q_2^+ mode, a columnar orbital pattern is stabilized instead of the checkerboard pattern associated with the JT effect. Consequently, super-exchange paths are enabled along the z axis thereby creating AFM interactions along the “columns”. Such a behavior is indeed verified in our simulations: when starting from a $(\sqrt{2}a, \sqrt{2}a, 2a)$ cubic cell of YVO_3 with specific initial electron nudging (similar to those presented in Section III.A), we find after variational self-consistency that the columnar orbital pattern is more stable than the checkerboard arrangement when considering the G-type AFM order ($\Delta E_{\text{che-col}} = +31$ meV/f.u), and conversely for the C-type AFM order ($\Delta E_{\text{che-col}} = -74$

meV/f.u). In other words, each Q_2 mode is associated to a specific orbital pattern, and consequently to a precise spin order.

Nevertheless, the checkerboard orbital pattern remains the global energy minimum in the cubic cell (between the G and C type AFM orders), a similar conclusion being drawn with a FM order ($\Delta E_{\text{che-col}} = -34$ meV). Therefore, YVO_3 should exhibit the signature of a JT effect although the low T phase only shows the Q_2^+ mode. This is verified experimentally by the presence of an intermediate $P2_1/b$ symmetry characterized by the Q_2^- mode as shown by the symmetry adapted mode analysis presented in Table 1 of Ref.¹³. Thus, the question is now what is the driving force of the transition to the purely orthorhombic $Pbnm$ cell at 0 K for YVO_3 .

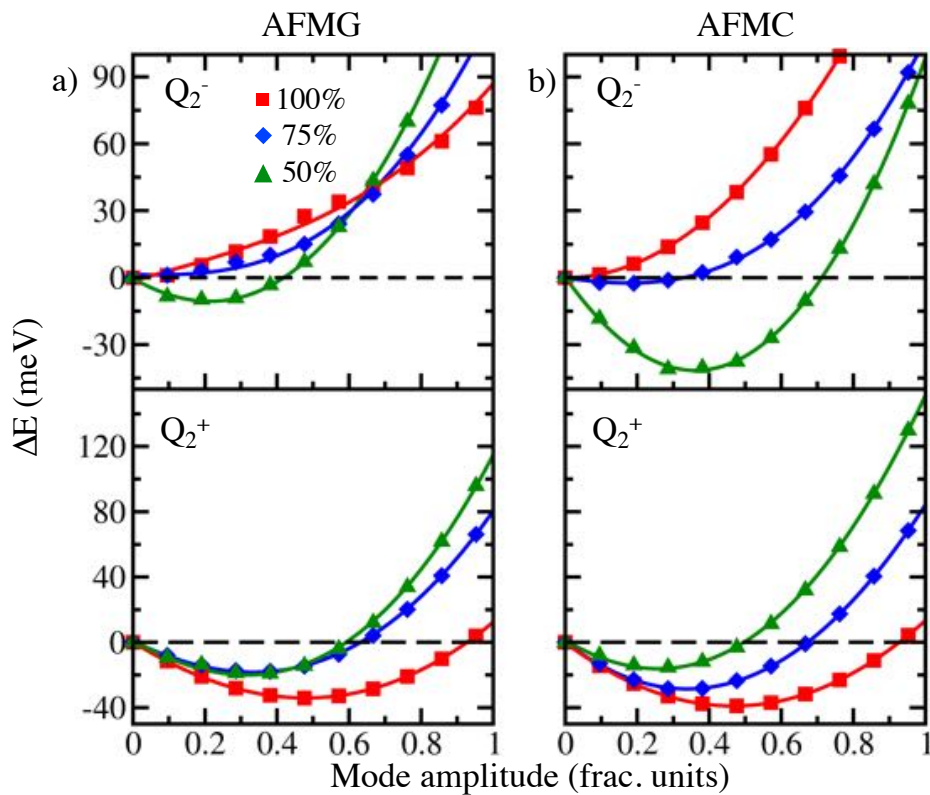


Figure 5: Energy difference (in meV per 20 atom unit cell) as a function of the Q_2^+ and Q_2^- mode amplitudes (in fractional units) at fixed rotation and antipolar displacement amplitude (in %) appearing in the ground state structure of YVO_3 using the AFMG (a) and AFMC (b) order. The unit cell is fixed to a $(\sqrt{2}a, \sqrt{2}a, 2a)$ cell whose lattice parameter yields the ground state volume. 1 is actually the amplitude appearing in the ground state structure.

To get insights on this peculiar transition, we start from the high symmetry $(\sqrt{2}a, \sqrt{2}a, 2a)$ cubic cell of YVO_3 and we freeze fixed amplitudes of all distortions appearing in the ground state structure except the Q_2^+ mode, *i.e.* add only octahedra rotations and antipolar motions of ions. Then, we compute the potential energy surface associated with Q_2^+ or Q_2^- modes (see Figure 5). Upon increasing “orthorhombic distortions”, two antagonist effects are observed irrespective of the AFMG or AFMC magnetic order: (i) the Q_2^+ mode describes a single well potential whose energy minimum is progressively shifted to larger amplitudes while (ii) the Q_2^- mode vanishes. The former observation is in line with the improper origin of the Q_2^+ distortion discussed in section C but the latter finding indicates that orthorhombic distortions produce a crystal field sufficient to split the t_{2g} level degeneracies³³ but also diminish electronic super exchange interaction at the core of the JT effect (see Supplementary Section VIII “Cooperating/competing octahedra rotations and Jahn-Teller effect in LaVO_3 ”).

Our results are closely compatible with the experimental phase diagram of rare-earth vanadates^{23,53} and settle the issue that Q_2^- and Q_2^+ have totally different origins, the former being the signature of the Jahn-Teller effect while the latter is just a consequence of the ubiquitous octahedra rotations appearing in perovskites. RVO_3 are then unique materials in the sense that they are the only oxide perovskites with B=3d element showing a JT effect plus the sterically induced Q_2^+ mode, thereby they are the only member possessing entangled spin-orbital properties.

IV. Conclusions

We have explained the modalities enabling a Jahn-Teller effect in ABX_3 perovskites and identified its signature: strongly localized electronic states are the key factor for a spontaneous electronic instability to produce a Jahn-Teller distortion with a specific octahedra deformation pattern that is experimentally detectable and detected. In materials with larger anions p and B cations d states hybridizations, there is no electronic instability that can break orbital degeneracies and the observed octahedra deformation has a distinct symmetry that is pushed by lattice mode couplings with rotations. The Q_2^+ octahedral

deformation, appearing in LaMnO₃ or LaTiO₃, is not induced by an electronic instability and thus it is not a Jahn-Teller distortion. It is a consequence of octahedral rotations and tilts often appearing in the perovskite oxides due to pure semiclassical atomic size effects, i.e. geometric steric effects.

Our work provides a single theory explaining the Jahn-Teller effect and its specific signatures and reconcile the numerous experimental results of ABX₃ materials studied to date. Last but not least, our results settle the fact that dynamical correlations, and the Mott-Hubbard model, are absolutely not an essential aspect of the physics of ABX₃ materials showing insulating states despite the presence of degenerate states in the parent cubic cell, thereby defining DFT as a sufficient platform to study the physics of ABX₃ materials.

Some details of the Method: DFT calculations are performed with the VASP package^{41,42} and electrons are nudged using the modified VASP routine⁴³. We used PAW potentials with the outer 4s, 4p and 3d B cation electrons explicitly treated in the simulations. 6*6*4 k-point mesh was used for the relaxation of the ($\sqrt{2}a$, $\sqrt{2}a$, 2a) cubic cells, increased to 8*8*6 for plotting energy potential surfaces and seeking for OBS, accompanied by an energy cut-off of 500 eV. Energy potential surfaces were plotted with symmetry of the wavefunction off, in order to allow electrons to occupy the lowest energy state.

Acknowledgments: This work of JV has been supported by the European Research Council (ERC) Consolidator grant MINT under the Contract No. 615759. Calculations took advantages of the Occigen machines through the DARI project EPOC A0020910084 and of the DECI resource FIONN in Ireland at ICHEC through the PRACE project FiPSCO. The work of AZ was supported by Department of Energy, Office of Science, Basic Energy Science, MSE division under Grant No. DE-FG02-13ER46959 to CU Boulder. JV acknowledges support from A. Ralph at ICHEC supercomputers.

References

¹ H.K.D.R.Y.H.B. (Eds.), *The Jahn-Teller Effect Fundamentals and Implications for Physics and Chemistry* (2009).

² D.I. Khomskii, *Transition Metal Compounds*, Cambridge (2014).

³ J.B. Goodenough, *Annu. Rev. Mater. Sci.* **28**, 1 (1998).

- ⁴ V.M. Goldschmidt, *Naturwissenschaften* **14**, 477 (1926).
- ⁵ Y. Tokura and N. Nagaosa, *Science* **288**, 462 (2000).
- ⁶ H.A. Jahn and E. Teller, *Proc. R. Soc. London Ser. A - Math. Phys. Sci.* **161**, 220 (1937).
- ⁷ M. Baldini, V. V. Struzhkin, A.F. Goncharov, P. Postorino, and W.L. Mao, *Phys. Rev. Lett.* **106**, 064402 (2011).
- ⁸ N. Binggeli and M. Altarelli, *Phys. Rev. B* **70**, 085117 (2004).
- ⁹ E. Pavarini and E. Koch, *Phys. Rev. Lett.* **104**, 086402 (2010).
- ¹⁰ K.I. Kugel and D.I. Khomskii, *Sov. Phys. JETP* **64**, 1429 (1973).
- ¹¹ K.I. Kugel and D.I. Khomskii, *Sov. Phys. Usp.* **25**, 231 (1982).
- ¹² Y. Ren, T.T.M. Palstra, D.I. Khomskii, E. Pellegrin, A.A. Nugroho, A.A. Menovsky, and G.A. Sawatzky, *Nature* **396**, 441 (1998).
- ¹³ J. Varignon, N.C. Bristowe, E. Bousquet, and P. Ghosez, *Sci. Rep.* **5**, 15364 (2015).
- ¹⁴ J. Varignon, N.C. Bristowe, and P. Ghosez, *Phys. Rev. Lett.* **116**, 57602 (2016).
- ¹⁵ A. Stroppa, P. Barone, P. Jain, J. M. Perez-Mato, and S. Picozzi, *Adv. Mater.* **25**, 2284 (2013).
- ¹⁶ A. Stroppa, P. Jain, P. Barone, M. Marsman, J.M. Perez-Mato, A.K. Cheetham, H.W. Kroto, and S. Picozzi, *Angew. Chemie - Int. Ed.* **50**, 5847 (2011).
- ¹⁷ J. Chaloupka and G. Khaliullin, *Phys. Rev. Lett.* **100**, 16404 (2008).
- ¹⁸ D. Kumar, A. David, A. Fouchet, A. Pautrat, J. Varignon, C.U. Jung, U. Lüders, B. Domengès, O. Copie, P. Ghosez, and W. Prellier, **99**, 224405 (2019).
- ¹⁹ Y. Zhang, M.M. Schmitt, A. Mercy, J. Wang, and P. Ghosez, *Phys. Rev. B* **98**, 081108(R) (2018).
- ²⁰ S. Margadonna and G. Karotsis, *J. Am. Chem. Soc.* **128**, 16436 (2006).
- ²¹ A. Okazaki and Y. Suemune, *J. Phys. Soc. Jpn* **16**, 176 (1961).
- ²² J. Rodriguez-Carvajal, M. Hennion, F. Moussa, and A.H. Moudden, *Phys. Rev. B.* **57**, 3189 (1998).
- ²³ M.H. Sage, G.R. Blake, C. Marquina, and T.T.M. Palstra, *Phys. Rev. B* **76**, 195102 (2007).
- ²⁴ Y. Yang, W. Ren, M. Stengel, X.H. Yan, and L. Bellaiche, *Phys. Rev. Lett.* **109**, 57602 (2012).
- ²⁵ E. Pavarini, E. Koch, and A.I. Lichtenstein, *Phys. Rev. Lett.* **101**, 266405 (2008).
- ²⁶ J. Varignon, M.N. Grisolia, D. Preziosi, P. Ghosez, and M. Bibes, *Phys. Rev. B* **96**, 235106 (2017).
- ²⁷ M.A. Carpenter and C.J. Howard, *Acta Crystallogr. Sect. B Struct. Sci.* **65**, 134 (2009).

- ²⁸ I. Leonov, D. Korotin, N. Binggeli, V.I. Anisimov, and D. Vollhardt, Phys. Rev. B **81**, 075109 (2010).
- ²⁹ I. Leonov, N. Binggeli, D. Korotin, V.I. Anisimov, N. Stojić, and D. Vollhardt, Phys. Rev. Lett. **101**, 096405 (2008).
- ³⁰ J. Varignon, M. Bibes, and A. Zunger, Phys. Rev. B **100**, 035119 (2019).
- ³¹ G. Trimarchi, Z. Wang, and A. Zunger, Phys. Rev. B **97**, 035107 (2018).
- ³² G.M. Dalpian, Q. Liu, J. Varignon, M. Bibes, and A. Zunger, Phys. Rev. B **98**, 075135 (2018).
- ³³ J. Varignon, M. Bibes, and A. Zunger, Nat. Commun. **10**, 1658 (2019).
- ³⁴ S. Xu, X. Shen, K.A. Hallman, R.F. Haglund, and S.T. Pantelides, Phys. Rev. B **95**, 125105 (2017).
- ³⁵ J.W. Furness, Y. Zhang, C. Lane, I.G. Buda, B. Barbiellini, R.S. Markiewicz, A. Bansil, and J. Sun, Commun. Phys. **1**, 11 (2018).
- ³⁶ C. Lane, J.W. Furness, I.G. Buda, Y. Zhang, R.S. Markiewicz, B. Barbiellini, J. Sun, and A. Bansil, Phys. Rev. B **98**, 125140 (2018).
- ³⁷ Q. Liu, Q. Yao, Z.A. Kelly, C.M. Pasco, T.M. McQueen, S. Lany, and A. Zunger, Phys. Rev. Lett. **121**, 186402 (2018).
- ³⁸ Q. Liu, G.M. Dalpian, and A. Zunger, Phys. Rev. Lett. **122**, 106403 (2019).
- ³⁹ J.M. Perez-Mato, D. Orobengoa, and M.I. Aroyo, Acta Crystallogr. Sect. A Found. Crystallogr. **66**, 558 (2010).
- ⁴⁰ D. Orobengoa, C. Capillas, I. Aroyo, and J.M. Perez, J. Appl. Crystallogr. **42**, 820 (2009).
- ⁴¹ G. Kresse and J. Hafner, Phys. Rev. B **47**, 558 (1993).
- ⁴² G. Kresse and J. Furthmüller, Comput. Mater. Sci. **6**, 15 (1996).
- ⁴³ J.P. Allen and G.W. Watson, Phys. Chem. Chem. Phys. **16**, 21016 (2014).
- ⁴⁴ J.P. Perdew, A. Ruzsinszky, G.I. Csonka, O.A. Vydrov, G.E. Scuseria, L.A. Constantin, X. Zhou, and K. Burke, Phys. Rev. Lett. **100**, 136406 (2008).
- ⁴⁵ S.L. Dudarev, S.Y. Savrasov, C.J. Humphreys, and a. P. Sutton, Phys. Rev. B **57**, 1505 (1998).
- ⁴⁶ J. Heyd, G.E. Scuseria, and M. Ernzerhof, J. Chem. Phys. **118**, 8207 (2003).
- ⁴⁷ A. V. Krugau, O.A. Vydrov, A.F. Izmaylov, and G.E. Scuseria, J. Chem. Phys. **125**, 224106 (2006).
- ⁴⁸ S. Miyasaka, J. Fujioka, M. Iwama, Y. Okimoto, and Y. Tokura, Phys. Rev. B - Condens. Matter Mater. Phys. **73**, 224436 (2006).

- ⁴⁹ G.A. Baraff, E.O. Kane, and M. Schlüter, Phys. Rev. B **21**, 5662 (1980).
- ⁵⁰ C. Autieri, E. Koch, and E. Pavarini, Phys. Rev. B **89**, 155109 (2014).
- ⁵¹ S. Margadonna and G. Karotsis, J. Mater. Chem. **17**, 2013 (2007).
- ⁵² L. Paolasini, R. Caciuffo, A. Sollier, P. Ghigna, and M. Altarelli, Phys. Rev. Lett. **88**, 106403 (2002).
- ⁵³ S. Miyasaka, Y. Okimoto, M. Iwama, and Y. Tokura, Phys. Rev. B **68**, 100406 (2003).
- ⁵⁴ M. Cwik, T. Lorenz, J. Baier, R. Müller, G. André, F. Bourée, F. Lichtenberg, A. Freimuth, R. Schmitz, E. Müller-Hartmann, and M. Braden, Phys. Rev. B **68**, 060401 (2003).
- ⁵⁵ P. Bordet, C. Chailout, M. Marezio, Q. Huang, A. Santoro, S.W. Cheong, H. Takagi, C.S. Oglesby, and B. Batlogg, J. Solid State Chem. **106**, 253 (1993).
- ⁵⁶ H. Seim and H. Fjellvag, Acta Chem. Scand. **52**, 1096 (1998).
- ⁵⁷ J.H. Lee, K.T. Delaney, E. Bousquet, N.A. Spaldin, and K.M. Rabe, Phys. Rev. B **88**, 174426 (2013).
- ⁵⁸ C.J. Fennie and K.M. Rabe, Phys. Rev. B **72**, 100103(R) (2005).
- ⁵⁹ E. Bousquet, M. Dawber, N. Stucki, C. Lichtensteiger, P. Hermet, S. Gariglio, J.M. Triscone, and P. Ghosez, Nature **452**, 732 (2008).
- ⁶⁰ J. Hemberger, H.K. Von Nidda, V. Fritsch, J. Deisenhofer, S. Lobina, T. Rudolf, and P. Lunkenheimer, Phys Rev Lett. **91**, 066403 (2003).
- ⁶¹ M. Cwik, T. Lorenz, J. Baier, R. Müller, G. André, F. Bourée, F. Lichtenberg, A. Freimuth, R. Schmitz, E. Müller-Hartmann, and M. Braden, Phys. Rev. B **68**, 060401 (2003).
- ⁶² X. Qiu, T. Proffen, J.F. Mitchell, and S.J.L. Billinge, Phys. Rev. Lett. **94**, 1 (2005).